Analytic expressions for the Dirac treatment of nucleon-nucleus scattering

R. D. Amado, J. Piekarewicz, and D. A. Sparrow
Department of Physics, University of Pennsylvania, Philadelphia, Pennsylvania 19104

J. A. McNeil
Department of Physics, Villanova University, Villanova, Pennsylvania 19085
(Received 3 October 1983)

We extend earlier work on analytic evaluations of nucleon scattering amplitudes to the Dirac treatment. The resulting closed form expressions are accurate and show how the two-body and target input influence scattering observables. The insight available should be quite useful as the Dirac equation description of proton-nucleus scattering becomes the standard approach.

I. INTRODUCTION

In this paper we extend earlier work on analytic evaluations of nucleon scattering amplitudes to particles described by the Dirac equation. The resulting closed form expressions are accurate and allow one to see by inspection how the two-body and target input influence scattering observables. The insight available should become increasingly useful as the Dirac equation description of proton-nucleus scattering becomes the standard approach. We first review the situation in nucleon-nucleus scattering.

At intermediate energy both the optical model (Kerman, McManus, and Thaler[1]) and the equivalent eikonal (Glauber[2]) treatments of hadron nucleus scattering have been quite successful at describing the general features of the cross sections, often yielding descriptions that are quite accurate in detail. These treatments are based on the Schrödinger equation and the impulse approximation. Amado, Dedonder, and Lenz[3] (ADL) have shown that the the eikonal integrals can be evaluated analytically in a systematic asymptotic treatment. The analytic treatment demonstrates explicitly in what way each of the target density and projectile-nucleon interaction variables affects the final cross section. The approach can be generalized to the inclusion of spin,[4,5] inelastic scattering[6] including spin,[7] and even coupled channels processes.[8] In addition to making manifest the connection between input variables and observable features of the scattering, the analytic approach allows for the derivation of data-to-data relationships directly connecting elastic and inelastic cross sections and spin observables.

Mathematically, the approach hinges on evaluating the integrals by the method of stationary phase. Physically, the simple results, and especially the data-to-data relationships, are due to distortion dominance. Thus far the algebra has been worked out only for distortion factors with a singularity arising from a simple pole in the density (Woods-Saxon form), with small corrections due to the spin-orbit force proportional to the derivative of the density. This has limited the application of the methods to Schrödinger treatments of proton scattering above around 200 MeV, where the spin orbit force is weak and can be treated perturbatively.

Recently, it has become clear that a treatment of proton scattering based on the impulse approximation and the Schrödinger equation is inadequate,[9,10] especially in the treatment of spin dependence.[5,10] Furthermore, it has been shown that phenomenological treatments based on the Dirac equation are very successful at describing the data.[11] Finally, an impulse approximation appropriate to the Dirac equation has been proposed[12] which describes all the essential features of the data.[13,14,10]

Against this backdrop, we have previously shown that the Dirac equation can be eikonalized in a way which respects the existence of both upper and lower components, and accurately reproduces exact partial wave solutions.[15] The resulting integral over impact parameters contains distortion terms proportional to the density squared, as well as to the density and its derivative. In Sec. II we will derive an analytic approximation to this integral, and in Sec. III show it to be very accurate for the parameters relevant to nucleon-nucleus scattering. This result contains the desired strong spin-orbit result for Schrödinger as well as Dirac particles. In Sec. IV we discuss the influence of the input parameters to the Dirac equation and contrast these with the Schrödinger case. A summary is presented in Sec. V.

II. ANALYTIC EVALUATION

We wish to evaluate the Dirac eikonal amplitude[15] for proton nucleus scattering analytically by using the method of stationary phase as in ADL. The major difference is that now there are three geometries and the evaluation is correspondingly more complicated. We begin by writing the scattering amplitude (still an operator in the 2×2 spin space) in the eikonal form[15]

$$T=-\frac{ik}{2\pi}\int d^2b\, e^{i\vec{q}\cdot\vec{b}}(e^{-X}-1)\,,$$
$$X=i\frac{m}{k}\int_{-\infty}^{\infty}dz\left[S+\frac{E}{m}V+\frac{S^2-V^2}{2m}\right]$$
$$-i\vec{\sigma}\cdot\frac{\hat{b}\times\hat{k}}{2}\int_{-\infty}^{\infty}\frac{(S'-V')}{E+m+S-V}dz\,, \tag{1}$$

where m is the proton mass, E its energy, and k its average wave number. The z direction is along $\vec{k}$ and $\vec{b}$ is the two-vector orthogonal to $\vec{k}$. S and V are the scalar and fourth component of vector potentials, respectively, assumed to be local and central, and hence to depend only on r. Primes denote differentiation with respect to r; $\vec{q}$ is the momentum transfer and is orthogonal to $\vec{k}$. The amplitude of Eq. (1) can be written as

$$T=T_0+\vec{\sigma}\cdot\hat{n}T_1 , \tag{2}$$

where

$$\hat{n}=\hat{q}\times\hat{k} ,$$

with

$$T_0=-ik\int_0^\infty b\,db\,J_0(qb)(e^{-X_1}\cosh X_2-1) , \tag{3a}$$

$$T_1=k\int_0^\infty b\,db\,J_1(qb)e^{-X_1}\sinh X_2 , \tag{3b}$$

with

$$X_1=i\frac{m}{k}\int_{-\infty}^{\infty}dz\left[S+\frac{E}{m}V+\frac{(S^2-V^2)}{2m}\right] , \tag{4a}$$

$$X_2=-\frac{i}{2}\int_{-\infty}^{\infty}dz\frac{(S'-V')}{E+m+S-V} . \tag{4b}$$

If we use

$$J_n(x)=\tfrac{1}{2}[H_n^{(1)}(x)+H_n^{(1)*}(x)] , \tag{5}$$

the exponential forms of cosh and sinh, and drop the 1 in (3a) that contributes only in the forward direction, we can write

$$T_0=-\frac{ik}{4}[G_0(q,X_1,X_2,1)+G_0(q,X_1,X_2,-1)+G_0^*(q,X_1^*,X_2^*,1)+G_0^*(q,X_1^*,X_2^*-1)] , \tag{6a}$$

$$T_1=-\frac{k}{4}[G_1(q,X_1,X_2,1)-G_1(q,X_1,X_2,-1)-G_1^*(q,X_1^*,X_2^*,1)+G_1^*(q,X_1^*,X_2^*,-1)] , \tag{6b}$$

in terms of the integral

$$G_n(q,X_1,X_2,\lambda)=\int_0^\infty b\,db\,H_n^{(1)}(qb)e^{-X_1+\lambda X_2} \tag{7}$$

(note that λ takes on the values ±1).

The G of (7) is a generalization of the G of Refs. 3–5. To evaluate the integral we go to large q where $H_n^{(1)}$ oscillates rapidly. That makes the integral a candidate for evaluation by the method of stationary phase. For large q we can use the asymptotic form of the Hankel function. Asymptotically,

$$H_1^{(1)}=-iH_0^{(1)} , \tag{8}$$

and, therefore, $G_1=-iG_0$ and we need only evaluate G_0. Using the asymptotic form for the Hankel function, we then have

$$G_0(q,X_1,X_2,\lambda)\cong\sqrt{2/\pi q}\,e^{-i(\pi/4)}\int_0^\infty\sqrt{b}\,db\,e^{g(b)} , \tag{9}$$

with

$$g(b)=iqb-X_1+\lambda X_2 . \tag{10}$$

The method of stationary phase consists in deforming the contour in (9) to find the point b_s where g is stationary (for distortion proportional to first or second powers of the density there is only one such point along the contour),

$$g'(b_s)=0 . \tag{11}$$

Expanding g about b_s, keeping only the quadratic term and doing the remaining integral as a Gaussian integral about b_s, yields

$$G_0(q,X_1,X_2,\lambda)=2\left[\frac{b_s}{-qg''(b_s)}\right]^{1/2}e^{-i(\pi/4)}e^{g(b_s)} , \tag{12}$$

where the condition for convergence of the Gaussian integral is $\mathrm{Re}\,g''<0$.

The remaining problem is to find b_s, $g(b_s)$, and $g''(b_s)$. We have already seen that most of the physics of Eq. (1) comes from assuming the same underlying density for V and S in a "$t\rho$" impulse approximation approach.[10] It is, therefore, that single underlying geometry case that we study here. In order to make contact with previous work, we take that density to have a Woods-Saxon or Fermi shape. It should be stressed, however, that this is a technically convenient assumption that is not crucial to the process.[16] We write

$$V=V_0f(r),\quad S=S_0f(r) ,\qquad f(r)=1/(1+e^{(r-c)/\beta}) , \tag{13}$$

where c is the half density radius and β the diffusivity. Inserting (13) in (4) we obtain for g of Eq. (10)

$$g(b)=iqb-i\frac{m}{k}\left[S_0+\frac{E}{m}V_0\right]\int_{-\infty}^{\infty}f\,dz-\frac{i}{2k}(S_0^2-V_0^2)\int_{-\infty}^{\infty}f^2dz+\frac{\lambda i}{2}\frac{(S_0-V_0)}{E+m}\int_{-\infty}^{\infty}dz\frac{f'}{1+\left[\frac{S_0-V_0}{E+m}\right]f} . \tag{14}$$

For large q, the first derivative of the first term grows, and hence to find b_s such that $g'(b_s)=0$, the derivative with respect to b of the other terms must grow as well. That is as q grows, b_s must approach a singular point of the integrals in (14). In G_0 the appropriate deformation of the integration contour is into the upper half-plane and in ADL it is

shown that the nearest singular point comes at $b=b_0=c+i\pi\beta$, which is also the singular point (a pole at $r=b_0$) of f. This is simply the statement that the dominant contribution to the integral comes from the surface since only there do the rapid oscillations of the integrand not cancel themselves out.

The details of evaluating the integrals in (14) near the singular point b_0 are presented in Appendix A. The result is

$$g(b)=iqb+\frac{i\alpha_1 b_0}{(b_0^2-b^2)^{1/2}}+\frac{i\alpha_2\beta b_0^2}{(b_0^2-b^2)^{3/2}}+\frac{i\alpha_2 b_0}{(b_0^2-b^2)^{1/2}}+\lambda\pi\left[\frac{b_0}{(b_0^2-b^2)^{1/2}}-\frac{B_0}{(B_0^2-b^2)^{1/2}}\right]$$
$$-\alpha_1\left[\frac{b_0}{2\pi\beta}\right]^{1/2}f_1-\alpha_2\left[\frac{b_0}{2\pi\beta}\right]^{1/2}f_2-\lambda\pi i\left[\left[\frac{B_0}{2\pi\beta}\right]^{1/2}-\left[\frac{b_0}{2\pi\beta}\right]^{1/2}\right]f_1\,, \tag{15}$$

where

$$\alpha_1=2\pi i\beta\frac{m}{k}\left[S_0+\frac{E}{m}V_0\right],$$
$$\alpha_2=2\pi i\beta\frac{m}{k}\left[\frac{S_0^2-V_0^2}{2m}\right],$$
$$\delta=\frac{S_0-V_0}{E+m}\,.$$
$$B_0=b_0+\beta\ln(1+\delta)\,, \tag{16}$$
$$\alpha_3=-i\pi\ln(1+\delta)\cong-i\pi\frac{(S_0-V_0)}{E+m}\,,$$
$$f_1=\frac{1}{\pi^{1/2}}\int_0^\infty\frac{dx}{\sqrt{x}}\left[\frac{1}{1-e^x}+\frac{1}{x}\right]=1.460\cdots\,,$$
$$f_2=\frac{1}{\pi^{1/2}}\int_0^\infty\frac{dx}{\sqrt{x}}\left[\frac{1}{1-e^x}+\frac{1}{x}\right]^2=0.4209\cdots\,.$$

The terms involving f_1 and f_2 in (15) are the nonsingular parts of the integrals and the expression in (16) for f_1 and f_2 are to leading order in β/b_0. It is simple to trace the parts of (15) back to (4) or (1b). The terms in α_1 come from the central potential linear in S and V, the term in α_2 from the quadratic central terms, and the terms in λ from the spin orbit potential.

For many cases of interest $\delta\ll1$ and for q not too large we can expand (15) to lowest order in δ or α_3. We then obtain

$$g=iqb+i\alpha_1'\frac{b_0}{(b_0^2-b^2)^{1/2}}+i\alpha_2'\frac{b_0^3}{(b_0^2-b^2)^{3/2}}$$
$$-\left[\frac{b_0}{2\pi\beta}\right]^{1/2}\left[\left[\alpha_1-\frac{\lambda}{2}\frac{\beta}{b_0}\alpha_3\right]f_1+\alpha_2 f_2\right], \tag{17}$$

where

$$\alpha_1'=\alpha_1+\alpha_2+i\lambda\pi\delta\frac{\beta}{b_0}=\alpha_1+\alpha_2-\lambda\frac{\beta}{b_0}\alpha_3\,,$$
$$\alpha_2'=(\alpha_2-i\lambda\pi\delta)\frac{\beta}{b_0}=(\alpha_2+\lambda\alpha_3)\frac{\beta}{b_0}\,. \tag{18}$$

We now use (17) to try to find the stationary point, b_s. We have

$$g'(b_s)=0=iq+i\frac{\alpha_1' b_0 b_s}{(b_0^2-b_s^2)^{3/2}}+\frac{3i\alpha_2' b_0^3 b_s}{(b_0^2-b_s^2)^{5/2}}\,. \tag{19}$$

Since $b_s\simeq b_0$ for large q, we write

$$b_s=b_0\left[1-\frac{\Delta}{2}\right]$$

or (20)

$$(b_0^2-b_s^2)^{1/2}=b_0\Delta^{1/2}\text{ if }\Delta\ll1\,,$$

then neglecting terms of order $\Delta^{-1/2}$ (these are also neglected in ADL) we obtain

$$-qb_0=\frac{\alpha_1'+\frac{3}{8}\alpha_2'}{\Delta^{3/2}}+\frac{3\alpha_2'}{\Delta^{5/2}}\,. \tag{21}$$

For $\alpha_2'=0$ we recover the results of ADL,

$$\Delta=\left[-\frac{\alpha_1'}{qb_0}\right]^{2/3}\,. \tag{22a}$$

For qb_0 very large, the $\Delta^{5/2}$ term dominates and we have

$$\Delta=\left[-\frac{3\alpha_2'}{qb_0}\right]^{2/5}\,. \tag{22b}$$

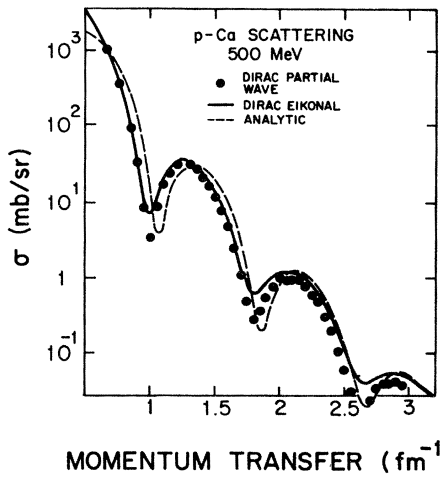

FIG. 1. Cross sections for 500 MeV n-^{40}Ca scattering, calculated using the exact Dirac equation ($\cdots$), the eikonal Dirac amplitude (——), and the analytic approximation to the eikonal Dirac amplitude (— — —) of this work.

TABLE I. Parameters for the Dirac equation.

		S_0 (MeV)	V_0 (MeV)	c (fm)	β (fm)
n-^{40}Ca	500 MeV	(−317.5,76.3)	(199.8,−88.5)	3.55	0.64
p-^{208}Pb	182 MeV	(−488.7,103.7)	(375.3,−115.3)	6.60	0.63
p-^{208}Pb	800 MeV	(−272.8,96.5)	(154.4,−109.0)	6.60	0.63

The actual case is intermediate and cannot be solved exactly. We have resorted to a numerical solution of the complex algebraic equation (21) always looking for roots that satisfy $\mathrm{Re}g''(b_s)<0$. In Appendix B we give a brief discussion of the general features of the roots of (21). Here, we simply note that for all phases of α_1' allowable by unitarity [$\mathrm{Re}(\alpha_1')>0$], and for any phase of α_2', the stationary phase point is between the singularity and the real axis, and there is only a single such stationary phase point satisfying $\mathrm{Re}[g''(b_s)]<0$.

The remaining ingredients of Eq. (12) are $g(b_s)$ and $g''(b_s)$. In terms of (17) and the solution of (21), these can be written

$$g(b_s)=iqb_0-\tfrac{3}{2}iqb_0\Delta-\frac{2i\alpha_2'}{\Delta^{3/2}} - \left[\frac{b_0}{2\pi\beta}\right]^{1/2}\left[\left[\alpha_1-\frac{\lambda\beta}{b_0}\alpha_3\right]f_1+\alpha_2 f_2\right]$$

and (23)

$$g''=\frac{3i}{\Delta b_0^2}\left[-qb_0+\frac{2i\alpha_2'}{\Delta^{5/2}}\right].$$

Before turning to an investigation of the numerical accuracy of our analytic forms it should be stressed that they represent a closed form, nonperturbative, unitary approximation to a scattering amplitude for the Dirac equation, and that approximation is the first term in a systematic development for which correction terms are easily obtained by the methods of ADL.

III. ACCURACY OF THE ANALYTIC METHOD

In this section we present comparison of exact partial wave, Dirac eikonal, and analytic expressions for the scattering observables. The first case considered is neutron scattering from ^{40}Ca at 500 MeV. This case was chosen since we have a direct numerical solution[17] of the Dirac equation for comparison. Cross sections, analyzing powers, and spin rotation functions are presented in Figs. 1–3, respectively, using the parameters given in Table I. In the description of the cross section all three are quite close for momentum transfers $0.5\le q\le 3.15$ fm^{-1}. The same is true for the analyzing power, although the analytic result gives minima which are too deep. For the spin rotation function the analytic method gives all the qualitative features and is quantitatively within ± 0.2 in the magnitude of Q. We present all three curves together to show that the analytic result agrees well with the direct partial wave solution as well as with the Dirac eikonal results.

To present a more complete picture, we have also prepared comparisons of eikonal and analytic treatments of proton scattering from ^{208}Pb at 182 and 800 MeV. These values nearly span the medium energy regime, and were chosen in part because data exist. Coulomb is included in the calculations. We see that beyond about 1 fm^{-1} there is good agreement for cross sections, asymmetries, and spin rotations at both energies (Figs. 4–6, respectively). The parameters given in Table I are from the impulse approximation. (These lead to a reasonable Dirac equation description of the data at 800 MeV but not at 182 MeV. Since the impulse approximation potentials are deeper than the phenomenological potentials at low energies the analytics are shown to be accurate for a wider range of potential depths than is likely to be needed.) In short, the method seems quite accurate for physically relevant Dirac potential strengths for a wide range of energies and nuclear masses. The analytic formalism is easily accurate enough to reveal the large difference in spin observables between the Dirac and Schrödinger approaches shown in Ref. 10 and Figs. 2 and 3. We turn now to some of the insights available through our approach.

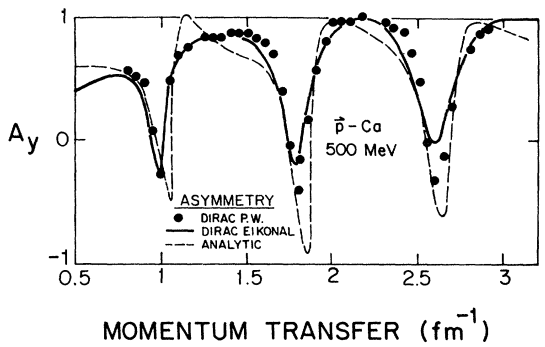

FIG. 2. Same as Fig. 1 for asymmetries.

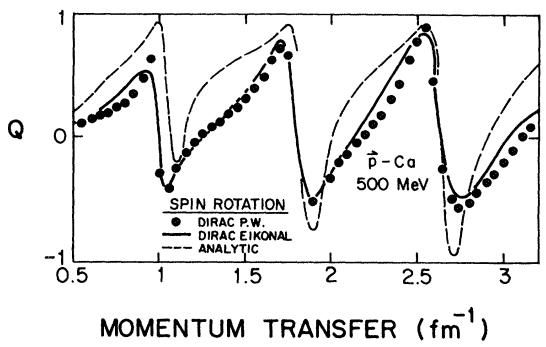

FIG. 3. Same as Fig. 1 for spin rotation.

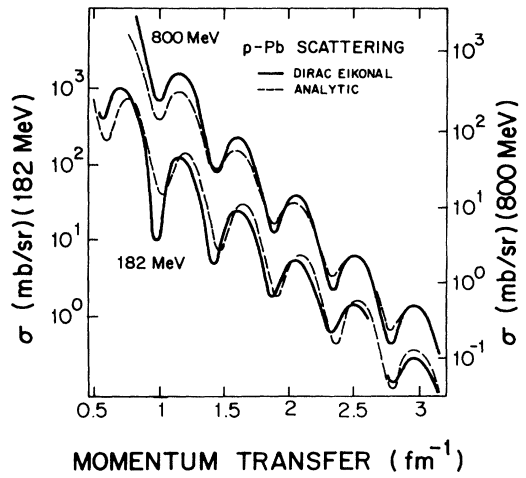

FIG. 4. Cross sections for p-^{208}Pb scattering at 182 and 800 MeV, calculated using the eikonal Dirac amplitude (——) and its analytic approximation (— — —) presented here.

IV. DISCUSSION OF THE SOLUTIONS

We have shown that the Dirac-eikonal scattering amplitude for nucleon-nucleus scattering can be analytically approximated very accurately for the range of parameters relevant to medium energy scattering. Now we would like to look at the solution in more detail. First, for simplicity, we may neglect spin and consider a potential in X of Eq. (1) of the form

$$V(r)=V_1 f(r)+V_2 f^2(r)\ ,$$

where

$$f(r)=1/(1+e^{(r-c)/\beta})\ .$$

In Eq. (18), α_1 and α_2 would be proportional to V_1 and V_2, respectively, α_1' to the sum V_1+V_2, and α_2' to β/b_0V_2. We illustrate in Fig. 7 the dependence of the stationary phase point on V_1 and V_2 by plotting the stationary phase point as a function of momentum transfer for $V_1=-i50$ MeV, $V_2=0$ (dark circles), and $V_1=0$, $V_2=-i50$ MeV (open circles), using $c=3.55$ fm and

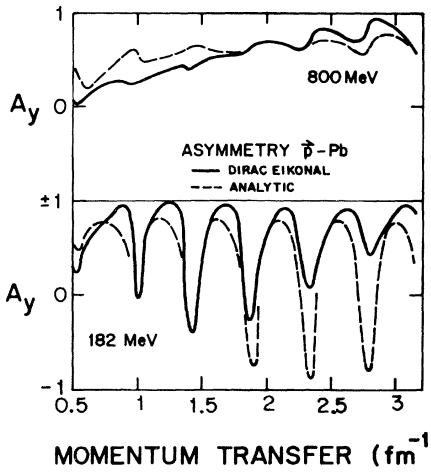

FIG. 5. Same as Fig. 4 for asymmetries.

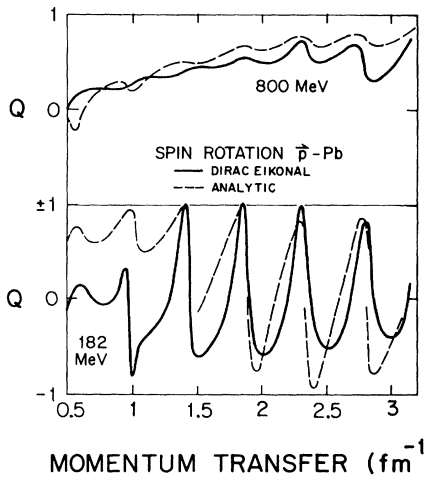

FIG. 6. Same as Fig. 4 for spin rotations.

$\beta=0.65$ fm for the density. The dashed and solid lines are the trajectories of the stationary phase point as a function of q [Eq. (17)] for the purely $(b_0^2-b^2)^{-1/2}$ and $(b_0^2-b^2)^{-3/2}$ singularities, respectively. For Vf interactions, the stationary phase point follows the trajectory associated with the $(b_0^2-b^2)^{-1/2}$ singularity alone since only that singularity is present for linear potentials. For Vf^2 interactions, both $(b_0^2-b^2)^{-1/2}$ and $(b_0^2-b^2)^{-3/2}$ singularities are present so the stationary phase point moves from some value intermediate to the purely $(b_0^2-b^2)^{-1/2}$ and $(b_0^2-b^2)^{-3/2}$ trajectories at low q to the purely $(b_0^2-b^2)^{-3/2}$ value for large q. Thus, we conclude that at low momentum transfers one probes the sum of linear and quadratic pieces while at higher momentum

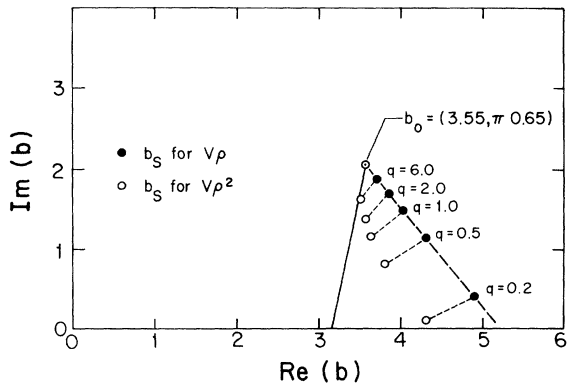

FIG. 7. Positions of the stationary phase point (fm) as a function of momentum transfer (fm^{-1}) for purely linear and purely quadratic interactions. The dashed line is the trajectory of the stationary phase point for

$$g\simeq iqb+i\alpha_1' b_0/(b_0^2-b^2)^{1/2}$$

in Eq. (17), and the solid line for

$$g=iqb+i\alpha_2' b_0^3/(b_0^2-b^2)^{-3/2}$$

in Eq. (17). For higher momentum transfer the stationary phase point b_s for the Vf^2 potential [which contains both $(b_0^2-b^2)^{-1/2}$ and $(b_0^2-b^2)^{-3/2}$ singularities] approaches the $(b_0^2-b^2)^{-3/2}$ lines.

TABLE II. Dimensionless measures of the interaction strengths for linear central, quadratic central, spin orbit, and total central interactions as a function of energy for the Schrödinger and Dirac impulse approximations.

T_{lab}	α_1	α_2	α_3	α_1'
200 MeV Schrödinger	(1.059,−0.968)	(0.000,0.000)	(0.253,1.189)	(1.059,−0.968)
Dirac	(1.057,−0.975)	(0.230,1.564)	(0.331,1.307)	(1.287,0.589)
300 MeV Schrödinger	(0.975,−0.485)	(0.000,0.000)	(0.223,0.938)	(0.975,−0.485)
Dirac	(0.973,−0.491)	(0.179,1.013)	(0.271,1.006)	(1.153,0.521)
400 MeV Schrödinger	(0.953,−0.284)	(0.000,0.000)	(0.206,0.778)	(0.953,−0.284)
Dirac	(0.951,−0.289)	(0.141,0.739)	(0.231,0.816)	(1.092,0.450)
500 MeV Schrödinger	(1.026,−0.187)	(0.000,0.000)	(0.211,0.664)	(1.026,−0.187)
Dirac	(1.023,−0.193)	(0.121,0.578)	(0.218,0.684)	(1.144,0.386)
600 MeV Schrödinger	(1.151,−0.091)	(0.000,0.000)	(0.225,0.582)	(1.151,−0.091)
Dirac	(1.148,−0.096)	(0.109,0.464)	(0.218,0.586)	(1.257,0.368)
700 MeV Schrödinger	(1.297,0.027)	(0.000,0.000)	(0.249,0.529)	(1.297,0.027)
Dirac	(1.294,0.022)	(0.123,0.395)	(0.237,0.526)	(1.416,0.417)
800 MeV Schrödinger	(1.358,0.174)	(0.000,0.000)	(0.260,0.505)	(1.358,0.174)
Dirac	(1.355,0.169)	(0.130,0.364)	(0.241,0.501)	(1.485,0.534)

transfers the quadratic piece alone increasingly asserts itself. Incidently, it is this interplay of linear and quadratic forms that has led to the "wine bottle" shape in Schrödinger phenomenology.

In another application we may use the analytic results to compare the features of the conventional Schrödinger impulse approximation with the Dirac impulse approximation. Looking at Eqs. (17) and (18) we see that what we should compare are the dimensionless strengths α_1, α_2, and α_3. For the Schrödinger case $\alpha_2=0$, so there is one appreciable difference right away. In Table II we present α_1, α_2, α_3, and α_1' for Schrödinger and Dirac impulse approximations for nucleon scattering from a $T=0$ nucleus. We see that α_1 and α_3, which come fairly directly from the forward nucleon-nucleon amplitude, are fairly similar throughout the medium energy regime. However, it is α_1' and α_2 which determine the central strength, and these are quite different. In fact, we find that up until 700 MeV the Schrödinger α_1' is effectively attractive (negative imaginary part) while for the Dirac it is effectively repulsive (positive imaginary part). Since it is the size of the imaginary part which determines minimum filling, this means that errors in descriptions of the minima which are usually down played may actually be quite significant. The superiority of the Dirac equation approach for the spin observables at high momentum transfer hinges upon the presence of an additional shape proportional to f^2. Here we see an opportunity to compare the Schrödinger and Dirac impulse approximations in terms of their predictions for the spin averaged cross sections.

Such a comparison cannot be made without including Coulomb effects. If we consider 500 MeV Schrödinger proton scattering we would expect the repulsive Coulomb interaction to largely cancel the strong attraction leading to deep minima. The value of q for which the cancellation would be maxima would tend to increase with A as the Coulomb gets relatively stronger. These are exactly the features exhibited by the Schrödinger calculations in Fig. 1 of Ref. 9.

The minima in the data presented there are, however, much shallower, indicating either a repulsive or a much less attractive interaction than predicted by the Schrödinger impulse approximation. The ^{208}Pb case best illustrates this point—the calculations show minima getting deeper with q whereas the experimental minima progressively fill with q.

This discussion suggests that Coulomb-nuclear interference type measurements could be carried out at any momentum transfer range to determine the effective value of the real part of the strong interaction. Such a determination would shed light on the validity of the impulse approximation and the various approaches based on it.

V. SUMMARY

In this paper we have derived an asymptotic analytic expression for the scattering of Dirac particles. The approach is numerically accurate over the entire medium energy range. Examining the form of the solutions shows that at low momentum transfer the quadratic forms in the interaction are at best marginally distinguishable from linear terms of the same central depth, but actually come to dominate at high momentum transfer. The solutions highlight the importance of a particular difference in the Schrödinger versus Dirac impulse approximations, namely the size (and often the sign) of the real part of the strong interaction. We hope that the analytic expressions presented here will lead to many further insights into the nature of the scattering of Dirac particles and make possible better connections between scattering at different energies and with different projectiles. We are currently work-

ing on the data to data approach to this problem.

We again express thanks to Professor B. C. Clark for the use of her calculations. We acknowledge financial support of the National Science Foundation.

APPENDIX A: SINGULAR PARTS OF PROFILE FUNCTIONS

To go from (14) to (15) we need to evaluate the integrals in (14) near the singular point b_0. We follow a generalization of the methods of ADL. First we note that $f(r)$ has a simple pole at $r=b_0$ with residue $-\beta$. In the upper half b plane near $b=b_0$, the singular part of f, f_0 can be written

$$f_0=\frac{-2\beta b_0}{r^2-b_0^2} . \tag{A1}$$

The first integral we encounter is precisely the one from ADL. Introducing f_0 we can write

$$\int_{-\infty}^{\infty} f(r)dz=\int_{-\infty}^{\infty}[f(r)-f_0]dz+\int_{-\infty}^{\infty} f_0 dz . \tag{A2}$$

Using $r^2=b^2+z^2$, the second term on the right in (A2), the singular term, is easily evaluated to yield

$$\int_{-\infty}^{\infty} f_0 dz=\frac{-2\pi i\beta b_0}{(b_0^2-b^2)^{1/2}},\quad \mathrm{Im}(b_0^2-b^2)^{1/2}>0 . \tag{A3}$$

The first term on the right of (A2), the nonsingular piece, may be written as

$$2\int_0^{\infty} dz\left[\frac{1}{1+e^{(r-c)/\beta}}+\frac{2\beta b_0}{z^2-b_0^2+b^2}\right] . \tag{A4}$$

Changing variables to x,

$$\beta x+b_0=(z^2+b^2)^{1/2}$$

and then evaluating the integral at $b=b_0$, since it is no longer singular, yields for (A4),

$$(2\beta b_0)^{1/2}\int_0^{\infty}\frac{dx}{\sqrt{x}}\frac{\left[1+\frac{\beta}{b_0}x\right]}{\left[1+\frac{\beta}{2b_0}x\right]^{1/2}} \times\left[\frac{1}{1-e^x}+\frac{1}{x\left[1+\frac{\beta}{2b_0}x\right]}\right] , \tag{A5}$$

or to leading order in β/b_0,

$$(2\pi\beta b_0)^{1/2}f_1 , \tag{A6}$$

with f_1 as given in (16).

We now generalize this method to the integral quadratic in f. We write

$$f^2=(f-f_0)^2+2f_0(f-f_0)+f_0^2 . \tag{A7}$$

The integral of the first term on the right is completely nonsingular and may be done as was done above for the nonsingular piece of the linear integral. Making the same substitution one obtains an expression just like (A5) but with the last bracket squared. To leading order in β/b_0 this yields $(2\pi b_0\beta)^{1/2}f_2$ as in (16). In the second term on the right-hand side in (A7) we may take the limit as $r\to b_0$ in $f-f_0$ before performing the z integer. As $r\to b_0$, $f-f_0\to\frac{1}{2}$ to leading order in β/b_0 and we obtain for the second term precisely the same integral as in (A3). The most singular term, the third on the right, is a trivial integral. All together we get for b near b_0

$$\int_{-\infty}^{\infty} f^2 dz=(2\pi\beta b_0)^{1/2}f_2-\frac{2\pi i\beta b_0}{(b_0^2-b^2)^{1/2}}-\frac{2\pi i\beta^2 b_0^2}{(b_0^2-b^2)^{3/2}};\quad \mathrm{Im}(b_0^2-b^2)^{1/2}>0 . \tag{A8}$$

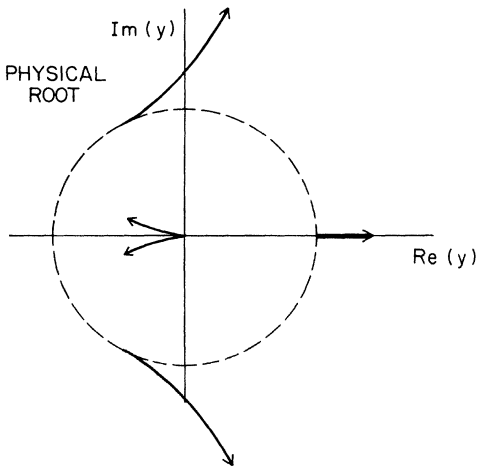

FIG. 8. Trajectory of the solutions of Eq. (B2) in the complex y plane.

We turn, finally, to the spin-orbit term, which we write as

$$\int dz\frac{f'}{\frac{1}{\delta}+f},\quad \delta=\frac{S_0-V_0}{E+m} . \tag{A9}$$

Differentiating f, we have for (A9)

$$-\frac{1}{\beta}\frac{\delta}{1+\delta}\int dz\frac{e^{(r-c)/\beta}}{(1+e^{(r-c)/\beta})}\left[1+\frac{1}{1+\delta}e^{(r-c)/\beta}\right]^{-1} =-\frac{1}{\beta}\int dz\left[\frac{1}{1+e^{(r-\bar{c})/\beta}}-\frac{1}{1+e^{(r-c)/\beta}}\right] , \tag{A10}$$

with $\bar{c}=c+\ln(1+\delta)$. These two integrals are each of the form of the integrals in (A2), yielding the result given in (15).

APPENDIX B: ROOTS

The stationary phase condition is given by Eq. (2), which we must solve for Δ the dimensionless measure of the distance from the stationary point to the singular point. With the variable substitution

$$x=\frac{3\alpha_2'}{(\alpha_1'+\frac{3}{8}\alpha_2')^{5/3}}(qb_0)^{2/3} \tag{B1a}$$

and

$$\Delta=\left[\frac{\alpha_1'+\frac{3}{8}\alpha_2'}{qb_0}\right]^{2/3} y\ , \tag{B1b}$$

Eq. (21) becomes

$$y^{5/2}+y+x=0\ . \tag{B2}$$

In this language small q is $x\to 0$ and large q is large x. Equation (B2) has five roots. As $x\to 0$, they are the three roots of $y^{3/2}=-1$ and two roots that vanish as $x\to 0$. The $e^{2/3\pi i}$ root of the first set is the ADL root. As $x\to\infty$, the five roots are the roots of $y^{5/2}=-x$, $y=x^{2/5i\pi(2n+1)}$, $n=0,1,2,3,4$.

Because of (B1b), even if y grows like $(qb_0)^{4/15}$, Δ decreases like $(qb_0)^{-2/5}$. For intermediate x the roots connect as shown in Fig. 8. For α_1' and α_2' predominantly real, the root that satisfies the condition $\mathrm{Im}(b_0^2-b^2)^{1/2}>0$ and $\mathrm{Re}g''(b_s)<0$ is the one that begins at $y=e^{2/3\pi i}$ for $x=0$ and goes to $y=x^{2/5}e^{2/5\pi i}$ for large x. In calculation, the root can be found by using an extrapolation formula, by using a prepared table, or by direct solution of (B2) or (21). In case of direct solution, care is required to ensure the correct root is chosen.

[1]A. K. Kerman, H. McManus, and R. M. Thaler, Ann. Phys. (N.Y.) 8, 551 (1959).

[2]R. J. Glauber, in *High Energy Physics and Nuclear Structure,* edited by G. Alexander (North-Holland, Amsterdam, 1967), p. 317.

[3]R. D. Amado, J. P. Dedonder, and F. Lenz, Phys. Rev. C 21, 647 (1980).

[4]R. D. Amado, J. A. McNeil, and D. A. Sparrow, Phys. Rev. C 23, 2114 (1981).

[5]J. A. McNeil, D. A. Sparrow, and R. D. Amado, Phys. Rev. C 26, 1141 (1982).

[6]R. D. Amado, F. Lenz, J. A. McNeil, and D. A. Sparrow, Phys. Rev. C 22, 2094 (1980).

[7]J. A. McNeil and D. A. Sparrow, Phys. Rev. C 23, 2124 (1981).

[8]R. D. Amado, J. A. McNeil, and D. A. Sparrow, Phys. Rev. C 23, 2186 (1981); 25, 13 (1982).

[9]G. W. Hoffman *et al.*, Phys. Rev. Lett. 47, 1436 (1981).

[10]R. D. Amado, J. Piekarewicz, D. A. Sparrow, and J. A. McNeil, Phys. Rev. C 28, 2180 (1983).

[11]L. G. Arnold, B. C. Clark, R. L. Mercer, and P. Schwandt, Phys. Rev. C 23, 1949 (1981); B. C. Clark, S. Hama, and R. L. Mercer, in Proceedings of the International Conference on Nuclear Structure, Amsterdam, 1982, and references contained therein.

[12]J. A. McNeil, J. R. Shepard, and S. J. Wallace, Phys. Rev. Lett. 50, 1439 (1983).

[13]J. R. Shepard, J. A. McNeil, and S. J. Wallace, Phys. Rev. Lett. 50, 1443 (1983).

[14]B. C. Clark *et al.*, submitted to Phys. Rev. Lett.

[15]R. D. Amado, J. Piekarewicz, D. A. Sparrow, and J. A. McNeil, Phys. Rev. C 28, 1663 (1983).

[16]H. E. Haber and D. A. Sparrow, Phys. Rev. C 25, 1959 (1982).

[17]B. C. Clark (private communication).